Journal of Extracellular Vesicles

RESEARCH ARTICLE OPEN ACCESS

Clinical Scale MSC-Derived Extracellular Vesicles Enhance Poststroke Neuroplasticity in Rodents and Non-Human Primates

Eun Hee Kim[1] | Jeong Pyo Son[2] | Gyun Sik Oh[1] | Suji Park[1] | Eunchong Hong[3] | Kyoung-Sun Lee[3] | Michael Chopp[4] | Oh Young Bang[1,5]

[1]S&E bio Co., Ltd., Seoul, South Korea | [2]Accelerator Radioisotope Research Section, Advanced Radiation Technology Institute (ARTI), Korea Atomic Energy Research Institute (KAERI), Jeongeup, South Korea | [3]Non-Clinical Evaluation Center (NCC), Osong Medical Innovation Foundation, Cheongju, South Korea | [4]Department of Neurology, Henry Ford Health, Detroit, Michigan, USA | [5]Sungkyunkwan University School of Medicine, Suwon, South Korea

Correspondence: Oh Young Bang (ohyoung.bang@samsung.com)

Received: 2 January 2025 | **Accepted:** 26 May 2025

Funding: S&E Bio, Inc. provided support for this study in the form of salaries for Eun Hee Kim, Gyun Sik Oh and Suji Park. The specific roles of these authors are articulated in the 'author contributions' section. This study was supported by a grant from the Technology Innovation Program (1415174804 and 20018049) funded by the Ministry of Trade, Industry & Energy (MOTIE, Korea). The funders had no role in study design, data collection and analysis, decision to publish, or preparation of the manuscript.

Keywords: extracellular vesicles | neurogenesis | primate | stem cells | stroke

ABSTRACT

Stroke is a leading cause of death and disability. The therapeutic potential of mesenchymal stem cell-derived extracellular vesicles (MSC-EVs) has shown considerable promise in rodent models of stroke. However, the therapeutic efficacy and safety of clinical-scale MSC-EVs for ischemic stroke are not well elucidated, especially in non-human primates. We developed a scalable production method for MSC-EVs using a 3D bioprocessing platform. EVs were isolated with a filter and tangential flow filtration and characterized using electron microscopy, nanoparticle tracking analysis, nanoflow cytometry analysis, proteomic and lipidomic analysis using mass spectrometry, and RNA sequencing. We determined the appropriate dosage and frequency of intravenous administration of EVs in a mouse stroke model. A biodistribution study of the selected dose regimen was performed using the internal cargo of EVs, human mitochondrial DNA. We then confirmed the efficacy of EVs in a marmoset stroke model. Improvement in behavioural tests and MRI-based neuroplasticity were compared between the control and EV groups through blinded evaluation. The proteome profiles of the infarcted hemisphere were also evaluated. EV products showed suitable lot-to-lot consistency. In a mouse stroke model, intravenous administration of a dose of 6×10^8 EVs for 5 days resulted in the smallest infarct volume and improvement in motor function. A biodistribution study showed that EVs were rapidly distributed into systemic organs and were relatively specifically distributed to the infarcted brain areas. Intravenous administration of an equivalent dose (3.5×10^9 EVs for 5 days) in a marmoset stroke model significantly improved motor functions and anatomical connectivity on diffusion MRI, and significantly reduced infarct volume. Proteomics analyses indicated that EV treatment promoted neurogenesis, synapse organization, and vascular development. In conclusion, this study is the first to demonstrate that a clinical-scale EV product is

Eun Hee Kim and Jeong Pyo Son contributed equally as the first authors.

This is an open access article under the terms of the Creative Commons Attribution-NonCommercial-NoDerivs License, which permits use and distribution in any medium, provided the original work is properly cited, the use is non-commercial and no modifications or adaptations are made.

© 2025 The Author(s). *Journal of Extracellular Vesicles* published by Wiley Periodicals LLC on behalf of International Society for Extracellular Vesicles.

safe and significantly enhances function recovery and neuroplasticity in a non-human primate stroke model, offering a promising treatment for human stroke.

1 | Introduction

Stroke is one of the leading causes of death and the most common cause of disability in adults. The approved treatments of acute ischaemic stroke are intravenous thrombolysis and thrombectomy. However, a substantial number of patients are ineligible for these recanalization therapies or remain in disabled status after treatment (Ribo et al. 2006; Molina 2010) requiring neuroprotective or neurovascular restorative strategies for patients with acute ischaemic stroke.

To date, all stroke neuroprotective agents have failed to translate to clinical human use, although most of them seemly effective in rodents (O'Collins et al. 2006). As a result, the current guidelines do not recommend the use of pharmacological agents with putative neuroprotective actions, except for research purposes (Powers et al. 2019). The STAIR (Stroke Treatment Academic Industry Roundtable) criteria provide guidelines aimed at making preclinical results more reflective of human stroke, and emphasize the importance of the quality of preclinical studies, because the possible reasons for loss in clinical translation include clinical trial design not matched to preclinical studies, and significant species differences (Dirnagl et al. 2013; Fisher 2011; Hossmann 2012). Non-human primates possess higher-order brains similar to humans and a rich behavioural repertoire amenable to assessments. Only a few preclinical studies of experimental treatment were conducted using stroke models of non-human primates. An exemplary case is the translation of NA-1, which targets postsynaptic density-95 protein to inhibit NMDA-mediated excitotoxic signalling following cerebral ischaemia (Tymianski 2011). The effect of NA-1 has been tested in non-human primates (macaques), and both MRI and behavioural assessments showed the beneficial effects of NA-1 in non-human primates (Cook et al. 2012). The translation of these results to humans has been reported, and in this randomized clinical trial, the same study protocol of the trial in non-human primates was used (Hill et al. 2020).

In recent years, extracellular vesicles (EVs) derived from mesenchymal stem cells (MSCs) have emerged as a promising cell-free therapeutic approach for stroke. These nano-sized vesicles carry bioactive molecules such as proteins, lipids and microRNAs that mediate the paracrine effects of MSCs, including anti-inflammatory responses, angiogenesis, neurogenesis and neuroprotection (Zhang et al. 2019). Preclinical studies in rodent models of stroke have demonstrated that MSC-EVs improve neurological function, reduce infarct size and enhance neuroplasticity through multiple mechanisms of action (Doeppner et al. 2015; Moon et al. 2019; Son et al. 2023; Xin et al. 2012).

In the present study, we hypothesised that a clinical scale mesenchymal stem cell-derived extracellular vesicle (MSC-EV) therapeutic improves behavioural functions, including hand functions and neuroplasticity after stroke, using neurological outcome measures and MRI measurements (including T_2-weighted MRI and diffusion tensor imaging [DTI]), respectively, following intravenous injections of an EV therapeutic after experimental stroke. To this end, we developed a three-dimensional (3D) bioprocessing platform designed using a cell non-adhesive microwell-patterned array for the scalable production of human Wharton's Jelly (WJ)-MSC-derived EVs with serum-free media (Son et al. 2023). First, to minimize the use of non-human primates in accordance with strengthened animal welfare principles, we initially compared the effects of different doses and frequencies of an EV product (code name, SNE-101) in a mouse model of stroke. Biodistribution studies of the selected dose regimen were performed using the internal cargo of EVs, human mitochondrial DNA (mtDNA). Based on these results, and to bridge the biological gap between rodents and humans, we then conducted experiments in non-human primates (marmosets), which bear genetic, anatomical and behavioural similarities to humans, using the same study protocol and the selected dose/frequency of SNE-101 administration. Lastly, imaging biomarker and proteomics analyses were performed to explore the potential mechanisms of action of SNE-101 in stroke recovery.

2 | Materials and Methods

All the tests were carried out and documented according to validated standard operating procedures. All research using human subjects was approved by the Institutional Review Board (*Samsung Medical Center Institutional Review Board*). WJ was obtained from three healthy volunteers. All volunteers or their named guardians provided written informed consent to participate in this study (IRB file No. 2016-07-102). Our research complied with the regulatory requirements for human cells, tissues and cellular and tissue-based products (HCT/Ps) regulated in compliance with Section CFR 1271 Title 21 '361' of PHS of US FDA. All animal experimental procedures were approved by the Institutional Animal Care and Use Committee (*Non-Clinical Evaluation Center; an AAALAC International approved facility*) of Osong Medical Innovation Foundation (protocol no. KBIO-IACUC-2023-055-1) and performed in accordance with the Animal Research: Reporting of In Vivo Experiments (ARRIVE) guidelines (Kilkenny et al. 2010). All animals were kept under the conditions of a temperature of 27°C ± 2°C, a relative humidity of 40% ± 10%, a lighting time of 12 h (7 AM to 7 PM), a ventilation frequency of 10 times/h, and an illuminance of 500 lux. All animals were observed twice daily for health monitoring, and no adverse events occurred.

2.1 | Preparation and Characterization of EVs

2.1.1 | Umbilical Cord Wharton's Jelly-Derived MSCs

We established master and working cell banks for consistency/reproducibility, quality control, and traceability/regulatory

20013078, 2025, 6, Downloaded from https://isevjournals.onlinelibrary.wiley.com/doi/10.1002/jev2.70110, Wiley Online Library on [13/01/2026]. See the Terms and Conditions (https://onlinelibrary.wiley.com/terms-and-conditions) on Wiley Online Library for rules of use; OA articles are governed by the applicable Creative Commons License

compliance for MSCs. The details of cell banking are described elsewhere (Son et al. 2023).

2.1.2 | Preparation of 3D Spheroid Culture of the WJ-MSCs

MSCs derived from human WJ of the umbilical cord (WJ-MSCs) were cultured at passage 8 in MEM Alpha minimum essential medium no phenol red (41061-029, Gibco, USA) supplemented with 10% FBS (16000-044, Gibco, USA) in a 5% CO_2 incubator at 37°C. At passage 9, WJ-MSCs were seeded into a micro-patterned well system (the EZSPHERE, ReproCELL Inc., Japan) containing approximately 69,000 microwells, each with a diameter and depth of 500 μm × 200 μm coated with 2-methacryloyloxyethyl phosphorylcholine polymer at a density of 400 cells/well to generate 3D spheroid culture in serum-free MEM Alpha minimum essential medium no phenol red. Spheroid cell aggregates were maintained uniformly in a micro-well system and cultured in CO_2 incubator at 37°C for a total of 4 days.

2.2 | Isolation of EVs

EV isolation was performed in a biological safety cabinet (BSC). Culture medium was collected by gentle pipetting at the top of the wells. To remove cell debris and apoptotic bodies, 1800 mL of culture medium was centrifuged at 2500 × *g* for 10 min, followed by filtration through a 0.22-μm membrane. The filtered media was separated using a 300-kDa MWCO mPES hollow fibre MiniKros filter module (Spectrum Laboratories, Rancho Dominguez, CA, USA) on a commercially available KrosFlo KR2I tangential flow filtration (TFF) system (Spectrum Laboratories, USA). After the TFF system, EVs were concentrated in phosphate-buffered saline (PBS) solution and filtered through a 0.22 μm membrane filter. EVs in PBS were stored at −80°C until use.

All processes were performed according to the current guidelines on quality, non-clinical and clinical assessment of EV therapy products of the Ministry of Food and Drug Safety (MFDS, released December 2018), and using GMP-compliant methods. The schematics for the processes of EV production, isolation, and quality control are shown in Figure S1.

2.3 | Characterisation of EVs

Following the guidelines recommended by the ISEV (International Society for Extracellular Vesicles), known as MISEV (Minimal Information for Studies of Extracellular Vesicles 2018 and 2023) and the Korean MFDS, the EVs isolated from the WJ-MSC cultured medium were characterised in terms of morphology, size distribution, surface markers, purity, potency marker, efficacy and safety (Thery et al. 2018; Welsh 2024).

See Supplementary Data for detailed methods for nanoparticle tracking analysis (NTA), Western blot, transmission electron microscopy (TEM) and cryogenic electron microscopy (cryoEM), enzyme-linked immunosorbent assay (ELISA), MACSPlex, NanoFCM, proteomics, small RNA sequencing, lipidomics, and safety tests.

2.4 | Mouse Stroke Model

2.4.1 | PT-Stroke Models

In this study, a total of 92 mice were divided into 11 groups (a dose experiment of 4 groups and a dosing frequency experiment of 7 groups). The sample size for this study was determined by a power calculation based on our previous data from a mouse photothrombotic (PT) stroke model with MRI analysis and functional behavioural changes (Son et al. 2023). We calculated that a sample size of 6 per each group was sufficient to evaluate therapeutic efficacy at effect size (*f*) 0.685, power 0.8, and significance 0.05. We determined that a sample size of 8 animals per group was required, considering a dropout rate of 25% (mortality and poor quality of modelling). Thirteen mice were excluded due to poor quality of modelling. Therefore, a total 79 mice were randomly divided into 11 groups (dose experiment groups [PBS, low, middle, and high; $n = 8, 10, 9$ and 10], and dosing frequency experiment groups [PBS, 1, 2, 3, 4, 5 and 6 times; $n = 8, 5, 5, 6, 6, 7$ and 5]). During the dose experiment, 2 mice died, and 8 mice were excluded due to cage mixing. The final number of animals in dose experiment groups (PBS, low, middle and high) were $n = 6, 7, 7$ and 7, respectively.

Adult 8-week-old male C57BL/6N mice (Orient Bio Inc., Korea) were used in this study. PT stroke was induced in the right-hand sensorimotor cortex of the mice. Briefly, mice were anaesthetized via intraperitoneal injection of a mixture of xylazine (20 mg/kg, 192492, Bayer, UK) and ketamine (100 mg/kg, No1AX03, Yuhan Co., Korea). Mice were shaved with an electric clipper, and the scalp was opened to expose the skull. Mice were fixed in a stereotaxic apparatus (A200905151233, KOPF instruments, USA), and 30 mg/kg of rose bengal (198250, Sigma, Germany) solution dissolved in PBS was injected via the jugular vein. After 5 min, the DPSS green (532 nm) laser (GL532T3-150FC, Lasercentury, China) placed 2.5 mm to the right, 0.5 mm anterior and 1.3 cm superior to the bregma illuminated for 15 min.

2.5 | MRI Image Analysis

MRI was performed using a 7*T* small animal MRI scanner (Bruker Biospin 70/20 USR, Fällanden). T_2-weighted MRI was performed at 1 and 7 days after PT modelling. Mice were anaesthetized using 5% isoflurane and maintained on 1.5% isoflurane. T_2-weighted images were acquired using a turbo rapid acquisition with a refocusing echo (Turbo RARE) sequence with the following parameters: repetition time (TR)/echo time (TE) = 3000/30 ms, field of view = 16 × 8 mm^2, image matrix = 128 × 64, and in-plane resolution = 0.125 × 0.125 × 0.5 mm^3.

2.6 | Behaviour Test

To assess the loss and recovery of motor function, the ladder rung walking test was performed before PT modelling and 4, 7, 14, 21 and 28 days after PT modelling (Metz and Whishaw 2002). The ladder rung apparatus consisted of two side walls made of clear Plexiglas with a metal rung horizontal ladder that the animal walked across. Before PT modelling, mice were trained for 3 consecutive days. The ladder rung walking test was performed

20013078, 2025, 6, Downloaded from https://isevjournals.onlinelibrary.wiley.com/doi/10.1002/jev2.70110, Wiley Online Library on [13/01/2026]. See the Terms and Conditions (https://onlinelibrary.wiley.com/terms-and-conditions) on Wiley Online Library for rules of use; OA articles are governed by the applicable Creative Commons License

with three trials each day, and tests were video-recorded from an inferior view. Foot fault errors were analysed left forelimb paw in each trial. The foot fault error rate was calculated according to the equation, number of error steps/number of total steps × 100 (%).

To assess the asymmetrical forelimb use of mice, the cylinder test was performed before PT modelling and 4, 7, 14, 21 and 28 days after PT modelling (Hua et al. 2002). Mice were placed within an open-top glass cylinder and recorded from the low side for 20 min. Forelimb contacts while rearing were scored with a total of 20 contacts. Ipsilesional forelimb contact was calculated according to the equation. Number of ipsilesional forelimb touches/number of (ipsilesional forelimb touches + contralesional forelimb touches) × 100 (%).

2.7 | Immunofluorescent Staining

Twenty-eight days after PT modelling, brains of mice were analysed using immunofluorescent staining. Brain tissue was fixed with 4% PFA (PC2031-100-00, Biosesang, Korea) and washed with PBS, and then incubated in 30% sucrose in PBS for 48 h at 4°C. Brain samples embedded in OCT compound (4583, Sakura, USA) are cut into 10 μm thickness by cryosection and attached to a gelatine-coated slide. For DCX (doublecortin, immature progenitor neurone marker) and ki-67 (cell proliferation marker) staining, the section containing brain tissue of the (subventricular zone) SVG region was fixed with ice-cold 100% methanol for 10 min, permeabilized with 0.15% TX-100 in PBS for 30 min at room temperature, and blocked with 2% BSA in PBS for 1 h at room temperature. The section was incubated overnight with anti-DCX antibody (1:250, ab207175, Abcam, USA) and anti-Ki67 antibody (1:100, 14-5698-82, Thermo Fisher, USA) in PBS containing 5% horse serum and 1% BSA at 4°C. After incubation, they were triple washed in PBS and incubated with anti-rabbit IgG-AlexaFluor 594 (1:200, ab1500777, Abcam, USA) and anti-goat IgG-AlexaFluor 488 (1:200, ab150160, Abcam, USA) in PBS containing 5% horse serum and 1% BSA for 1 h at room temperature. Slides were covered with a cover slide in a mounting solution containing DAPI. Fluorescent images were captured using a fluorescence microscope (EVOS M5000, Thermo Fisher, USA), and double positively stained cells in the SVG region of the infarcted hemisphere were quantified using the QuPath 0.4.3 program.

2.8 | Biodistribution Study of EVs Using mtDNA

Recently, a novel quantitative polymerase chain reaction (qPCR)-based assay to detect unmodified EVs by targeting mitochondrial deoxyribonucleic acid (mtDNA) was introduced, which effectively determined the biodistribution of unmodified EVs with high sensitivity and reproducibility and without artefacts related to artificial labelling of EVs (Cho et al. 2024). mtDNA is a constituent of EVs, and specific mtDNA regions that exhibited homologous variations distinct from their rodent mtDNA counterparts fully established this analytical approach. This method avoids the overestimation observed in biodistribution studies by labelling EVs with fluorescent dyes.

A total of 30 mice were subjected to PT modelling. One day after PT modelling, T_2-weighted MRI was performed. EVs were administered via tail vein injection (quaque die) Q.D. for 5 consecutive days. At 5 and 15 min, and at 1, 24, 72 h after the last EV injection, mice were anaesthetized, and blood, heart, lung, liver, kidney, brain, and spleen were excised. Tissue samples were snap frozen and stored at −80°C until DNA extraction. The Maxwell 48 blood purification kit (AS1400, Promega, USA) was used to extract tissue DNA from animal tissues and EVs. The frozen tissue was thawed at 4°C for 5 h, and 25 mg was homogenized using Bertin Corp. (Parkway Rockville, USA). Subsequently, the extracted DNA was dissolved in DNase and ribonuclease free-H2O following the manufacturer's instructions.

mtDNA was detected by qPCR using the COX-2 gene of human mitochondrial DNA. Primer and probe sets were to detect the COX-2 gene forward 5'-GCCCGCCATCATCCTAGTC-3', reverse 5'-CGTTGACCTCGTCTGTTATGTAAAG-3', probe 5'-FAM-CATCGCCCTCCCATCCCTACGC-BHQ1-3'. A 10 μL PCR reaction mixture contained 5 μL FAST Advanced MasterMix (Thermo Fisher Scientific), 0.9 μM of forward and reverse primers, 0.25 μM probe, and 1 μg amount of gDNA. qPCR reactions were performed using QuantStudio 7 Pro (Applied Biosystems, USA) with the following conditions: one cycle at 50°C for 2 min and 95°C for 10 min, followed by 40 cycles at 95°C for 15 s and 60°C for 1 min.

2.9 | Non-Human Primate Stroke Model

2.9.1 | Marmoset PT-Stroke Model

Adult laboratory-bred common marmoset monkeys (Callithrix jacchus), aged 30 to 136 months and weighing between 300 and 450 g, were utilized in this study. Based on comparative ageing studies (Tardif et al. 2011), this age range in marmosets approximately corresponds to human ages of 12 to 66 years, covering adolescents to older adults, and is clinically relevant to the age range of stroke patients. Focal cerebral ischaemia was induced in the marmosets via PT of microvessels using Rose Bengal (Sigma-Aldrich, St. Louis, MO, USA) (Le Friec et al. 2021). Anaesthesia was administered via intramuscular injection with 10 mg/kg ketamine hydrochloride (Yuhan Ketamine 50 Inj., Yuhan Corp, Seoul, Korea) and 0.5 mg/kg Atropine sulphate hydrate (Jeil Atropine Sulfate, Jeil Pharmaceutical, Seoul, Korea). Anaesthesia was maintained using a gas mixture of 2% isoflurane and oxygen delivered at a rate of 1 L/min through a nose cone.

During behavioural assessment training, the dominant forelimb was recorded, and based on this, photothrombotic ischaemic lesions were induced in the left hemisphere, as all animals exhibited right forelimb dominance. Skulls were secured using a stereotaxic apparatus, and a 6 mm diameter hole was drilled at coordinates 4.32 mm anterior from bregma and 3.85 mm lateral to the midline. Intravenous administration of 20 mg/mL Rose Bengal solution (20 mg/kg) was followed by 10 min of exposure to green laser light (GL532T3-150FC, Laser Century, Shanghai, China) at the skull perforation site, with precautions taken to prevent damage to surrounding tissues.

20013078, 2025, 6, Downloaded from https://isevjournals.onlinelibrary.wiley.com/doi/10.1002/jev2.70110, Wiley Online Library on [13/01/2026]. See the Terms and Conditions (https://onlinelibrary.wiley.com/terms-and-conditions) on Wiley Online Library for rules of use; OA articles are governed by the applicable Creative Commons License

Post-laser treatment, the skull piece covering the perforation site was reattached and fixed with dental cement, and the surgical site was sutured and disinfected with povidone. Continuous monitoring of heart rate, respiratory rate, and body temperature was maintained throughout the surgical procedure. To ensure the animals' well-being and recovery, we conducted daily observations and povidone wound disinfection for the first 5 days post-surgery, and administered pain relievers (Meloxicam [0.3 mg/kg, Metacam, Boehringer Ingelheim Vetmedica GmbH, Germany]) and an antibiotic (Baytril [5 mg/kg, Baytril, Bayer, Leverkusen, Germany]).

2.10 | Experimental Groups and Administration of EVs

A total of 12 marmoset monkeys, comprising 6 males and 6 females, were employed to establish a cerebral ischaemia model. Two female marmosets were excluded from the study for specific reasons: one was excluded due to a failure in the intravenous administration of the Rose Bengal solution, resulting in an infarct size significantly smaller than the average; the other was excluded due to limitations in behavioural assessments caused by tail necrosis. Consequently, the remaining 10 animals (6 males and 4 females) were randomly assigned to the EV group or the PBS control group, with each group consisting of 3 males and 2 females to ensure balanced sex distribution. One group received intravenous infusions of EVs (EV group, $n = 5$), and the other received PBS (control group, $n = 5$).

To evaluate the potential influence of sex and age on infarct severity, we conducted additional analyses. No significant difference in baseline infarct volume (Day 1 poststroke) was observed between male and female marmosets (unpaired t-test, $p = 0.8275$), nor between treatment groups (PBS vs. EV, $p = 0.5359$). In addition, no significant correlation was found between animal age and infarct volume (Pearson correlation, $r = 0.1823$, $p = 0.6141$), suggesting that neither sex nor age confounded the lesion size at baseline.

EVs or PBS were administered daily for 5 consecutive days, beginning the day after photothrombosis, via the tail vein.

2.11 | MRI Image Analysis

MRI was performed using a 4.7T small animal MRI scanner (Bruker Biospin 47/40 USR, Fällanden, Switzerland). A quadrature birdcage coil (inner diameter = 72 mm) was used for signal excitation and reception. MRI, including T_2-weighted imaging and DTI, was performed at 1, 7, and 28 days after PT stroke, under anaesthesia induced using isoflurane (5% for induction and 1.5% for maintenance). During MRI acquisition, the respiratory rate, heart rate, and body temperature of the animals were maintained and monitored using an animal monitoring-gating system (SA instruments, Stony Brook, NY, USA) and a warm bed. All MRI data were analysed by researchers blinded to the treatment information. The details of the methods for infarct volume measurement using T_2-weighted imaging analysis and brain microstructural changes using DTI data are described in Supplementary Data.

2.12 | Functional Behavioural Assessment

All behavioural tests, including modified neurological severity score (mNSS) assessment, grip test, and hill and valley staircase test, were conducted by a single observer blinded to the treatment conditions before and for up to 4 weeks after stroke induction (Tables S1–S3). The details of the marmoset behavioural tests are described in Supplementary Data and elsewhere (Le Friec et al. 2021).

2.13 | Haematological and Biochemical Analysis

A total of 1 mL of blood was obtained twice from the femoral vein prior to stroke modelling and euthanization. For haematological analysis, blood samples of 400 μL were collected in 1 mL tubes containing EDTA-K2 anticoagulant (BD Biosciences, NJ, USA), and automated haemogram tests were performed with an ADVIA 2120i haematology analyser (Siemens Healthineers, Erlangen, Germany). Whole blood cell analysis was conducted with 600 μL of blood collected in SST tubes (BD Biosciences, NJ, USA), which were allowed to fully coagulate, centrifuged at 5000 rpm for 10 min, and then analysed automatically using a Konelab 60i biochemical analyser (Thermo Fisher Scientific, MA, USA).

2.14 | Proteomics Analysis

Marmoset brain tissue was collected 28 days after PT stroke induction, proteins were isolated, and analysed by LC-MS/MS after TMT labelled and peptide fractionation. The detailed methods for the marmoset proteomics analyses are described in Supplementary Data.

2.15 | Statistical Analysis

Statistical analyses were performed using independent t-tests for infarct size analysis in the marmoset experiments, one-way analysis of variance (ANOVA) with Tukey's post hoc test for rodent dose-dependency and frequency experiments, and repeated measures ANOVA with Tukey's post hoc test for behavioural assessments. A threshold of p values below 0.05 were considered statistically significant. Graphs and statistical analyses were performed using GraphPad Prism 8 (GraphPad Software Inc.).

3 | Results

3.1 | EV Characterisation

EVs obtained from 3D spheroid culture (SNE-101) had a mean particle diameter of 158.17 ± 3.75 nm; the mode particle diameter was 147.83 ± 6.24 nm (Figure 1A), and exhibited a typical round shape on electron microscopy (TEM and Cryo-EM) (Figure 1B). To confirm the purity of EVs, the phospholipid membrane was stained with CMG dye, lysed with Triton X-100, a detergent, and the particles were measured by nanoparticle flow cytometry (nanoFCM). The percentage of particles stained by CMG was 94.9%, and among them, 97.9% were lysed by TX-100, confirming

20013078, 2025, 6, Downloaded from https://isevjournals.onlinelibrary.wiley.com/doi/10.1002/jev2.70110, Wiley Online Library on [13/01/2026]. See the Terms and Conditions (https://onlinelibrary.wiley.com/terms-and-conditions) on Wiley Online Library for rules of use; OA articles are governed by the applicable Creative Commons License

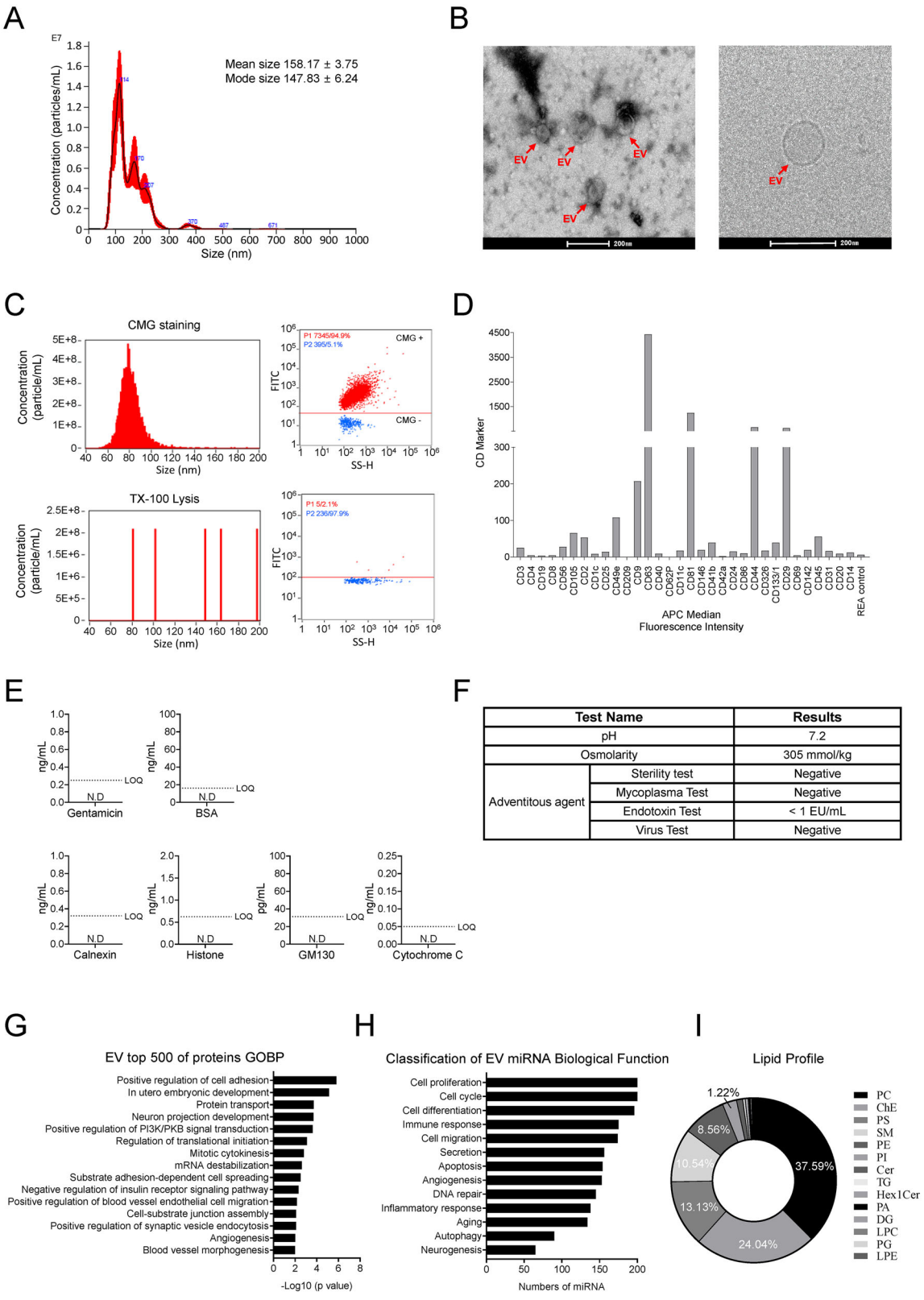

Test Name		Results
pH		7.2
Osmolarity		305 mmol/kg
Adventitous agent	Sterility test	Negative
	Mycoplasma Test	Negative
	Endotoxin Test	< 1 EU/mL
	Virus Test	Negative

FIGURE 1 | Characterization of extracellular vesicles (EVs). (A) A representative histogram for the distribution of the size of EVs using NanoSight. (B) Electron microscopic (EM) image of EVs acquired through transmission EM (TEM) (left panel) and cryo-EM (right panel). (C) EVs labelled with membrane-specific CMG dye were subjected to analysis via nanoparticle flow cytometry (nFCM) both prior to and subsequent to TX-100 treatment. Representative dot plots and particle size distribution histograms for CMG-labelled EVs (upper panel) and following TX-100 treatment (lower panel). (D) Surface marker expression profiling of EVs using multiplex bead-based flow cytometry. EV surface marker composition is shown after CD9/CD63/CD81-APC detection. (E) Evaluation of impurities present within EVs. The analysis of processing impurities (upper panel), including gentamicin and bovine serum albumin (BSA), was performed using ELISA kits. Cellular compartments, such as calnexin (endoplasmic reticulum protein), histone (nuclear protein), GM130 (Golgi apparatus protein) and cytochrome C (mitochondrial protein), were examined through ELISA kits (low panel). (F) Results of the

20013078, 2025, 6, Downloaded from https://isevjournals.onlinelibrary.wiley.com/doi/10.1002/jev2.70110, Wiley Online Library on [13/01/2026]. See the Terms and Conditions (https://onlinelibrary.wiley.com/terms-and-conditions) on Wiley Online Library for rules of use; OA articles are governed by the applicable Creative Commons License

pH, osmolarity and contaminant assessments of the EV solution. (G-I) Comprehensive multi-omics analysis of EV cargoes. (G) Gene Ontology Biological Process (GOBP) analysis utilizing EVs containing the top 500 proteins as identified through proteomics. (H) Classification of biological functions for EV miRNAs as identified by small RNA sequencing. (I) Lipidomic profiling of EVs. Data are expressed as mean ± standard deviation (SD) ($n = 3$). N.D, not detected.

that almost all particles were EVs (Figure 1C). We profiled EV surface antigens using a multiplex-bead-based flow cytometric assay. CD45, CD29, CD44, or CD105 indicated that they were of MSC origin, and CD81, CD63, or CD9 confirmed that they were EVs (Figure 1D). The particle per protein ratios of three different lots were similar, ranging from 3.45 to 4.56×10^8 particles/μg.

Gentamicin and bovine serum albumin (BSA), which are components of the 3D spheroid culture medium, were not detected in EVs, and none of the protein markers for identifying cell organelles, such as calnexin (ER marker), histone (nuclear marker), GM130 (Golgi marker), and cytochrome C (mitochondrial marker), were detected (Figure 1E). The pH, osmotic pressure, and safety corresponding to the general characteristics of the injection for EV administration in vivo were confirmed. The pH and osmotic pressure were 7.2 and 305 mmol/kg, respectively, which were levels suitable for in vivo administration, and no external contaminants were detected in the external contaminant tests (sterility, mycoplasma negativity test, external virus negativity test, and endotoxin) (Figure 1F).

Proteomics, small RNA sequencing, and lipidomics were performed to analyse the cargo of EVs. A total of 5452 proteins were identified in the proteome analysis, and Gene Ontology Biological Process (GOBP) analysis of 500 proteins with high expression confirmed that EVs are related to biological activities such as neurone projection development, angiogenesis, and blood vessel morphogenesis (Figure 1G). Small RNA sequencing identified 416 microRNAs (miRNAs), and these miRNAs were confirmed to be involved in various biological activities, including angiogenesis (153 miRNAs), neurogenesis (65 miRNAs), and immune response (175 miRNAs) (Figure 1H). Lipidomics analysis showed that phospholipids (PC, PS, SM, PE, PI) comprised the majority at 72.6% (37.6%, 13.1%, 10.5%, 8.6% and 2.8%, respectively), cholesterol ester comprised 24.0%, ceramide comprised 1.2%, and the rest comprised less than 1% (Figure 1I). EV products showed > 80% lot-to-lot consistency in the tested 3 lots in the proteomics, small RNAs, and lipidomics profiles (Figures S2–S4).

3.2 | Results of Rodent Study

3.2.1 | The Selection of Optimal Dose Regimen

In our previous study, we demonstrated that a single intravenous injection of EVs (6×10^8 particles/mouse) had a therapeutic effect in a mouse PT stroke model. To determine the optimal administration frequency, the same dose of EVs was administered once daily starting on Day 1 after stroke (Figures 2A–D). To evaluate the dose-dependency of EVs and identify the minimal effective dose, three different doses (low dose: 0.12×10^8 particles/mouse, medium dose: 6×10^8 particles/mouse, high dose: 300×10^8 particles/mouse) were administered intravenously on the same schedule (Figures 2E–H). Infarct size was measured using T_2-weighted MRI at Day 7 poststroke, behavioural changes were assessed by the ladder walk test and cylinder test up to 28 days poststroke, and the extent of brain tissue neurogenesis was determined by immunofluorescence analysis of the neurogenesis markers doublecortin (DCX) and Ki67 in the PT model animals at Day 28.

To optimize the treatment schedule, we compared the therapeutic efficacy in the PT model with increasing days of infusion of the medium dose (6×10^8/head) starting once a day. Mice receiving EVs for 5 days showed a significant decrease in infarct volume, improved behavioural performance, and increased DCX/Ki67 double-positive cell counts compared to the PBS group (Figures 2A–D). These results suggest that daily EV administration from Day 1 to 5 after stroke induction is the most effective treatment regimen. No significant improvement in infarct volume, behavioural recovery, or neurogenesis was observed in the low-dose group. In contrast, both the medium-dose and high-dose groups showed a significant decrease in infarct volume, improved functional recovery, and increased neurogenesis compared to the PBS group (Figures 2E–H). Moreover, there was a statistically significant difference in efficacy between the medium-dose and high-dose groups ($p < 0.05$ for all comparisons). This suggests a dose-dependent effect of EVs in the PT stroke model, with the medium dose being the minimally effective dose. Therefore, the optimal dose and administration frequency were selected as the intermediate dose once daily for a total of 5 times starting from the day after PT stroke induction.

3.2.2 | The Biodistribution of EVs in a Mouse Stroke Model

In this study, after the five daily intravenous administrations of the medium dose of EVs, the biodistribution of EVs was evaluated using detection of human mtDNA (Figure 2I). The (lower limit of quantification) LLOQ was confirmed to be 4.23 pg EV DNA/1 μg mouse DNA. LLOQ was not detected in mice that were not administered EVs (data not shown). In the PT model, DNA was extracted from the tissues 5 min, 1, 24 and 72 h after the fifth injection of EVs, and the mtDNA COX-2 gene was quantified to confirm the temporal profile distribution of EVs in each tissue. In the blood, the amount of mtDNA decreased over time after administration and was not detected at 72 h. In the brain, it was detected up to 1 h in the infarcted hemisphere, but not on the contralesional side. mtDNA was detected in the heart for up to 1 h but only at 5 min in other tissues, including the liver and lung. At 72 h, mtDNA was not detected in any of the tested organs. These findings indicate that EVs were primarily localized to the infarcted brain and that EVs were rapidly distributed into systemic organs and disappeared from most organs within 24 h.

20013078, 2025, 6, Downloaded from https://isevjournals.onlinelibrary.wiley.com/doi/10.1002/jev2.70110, Wiley Online Library on [13/01/2026]. See the Terms and Conditions (https://onlinelibrary.wiley.com/terms-and-conditions) on Wiley Online Library for rules of use; OA articles are governed by the applicable Creative Commons License

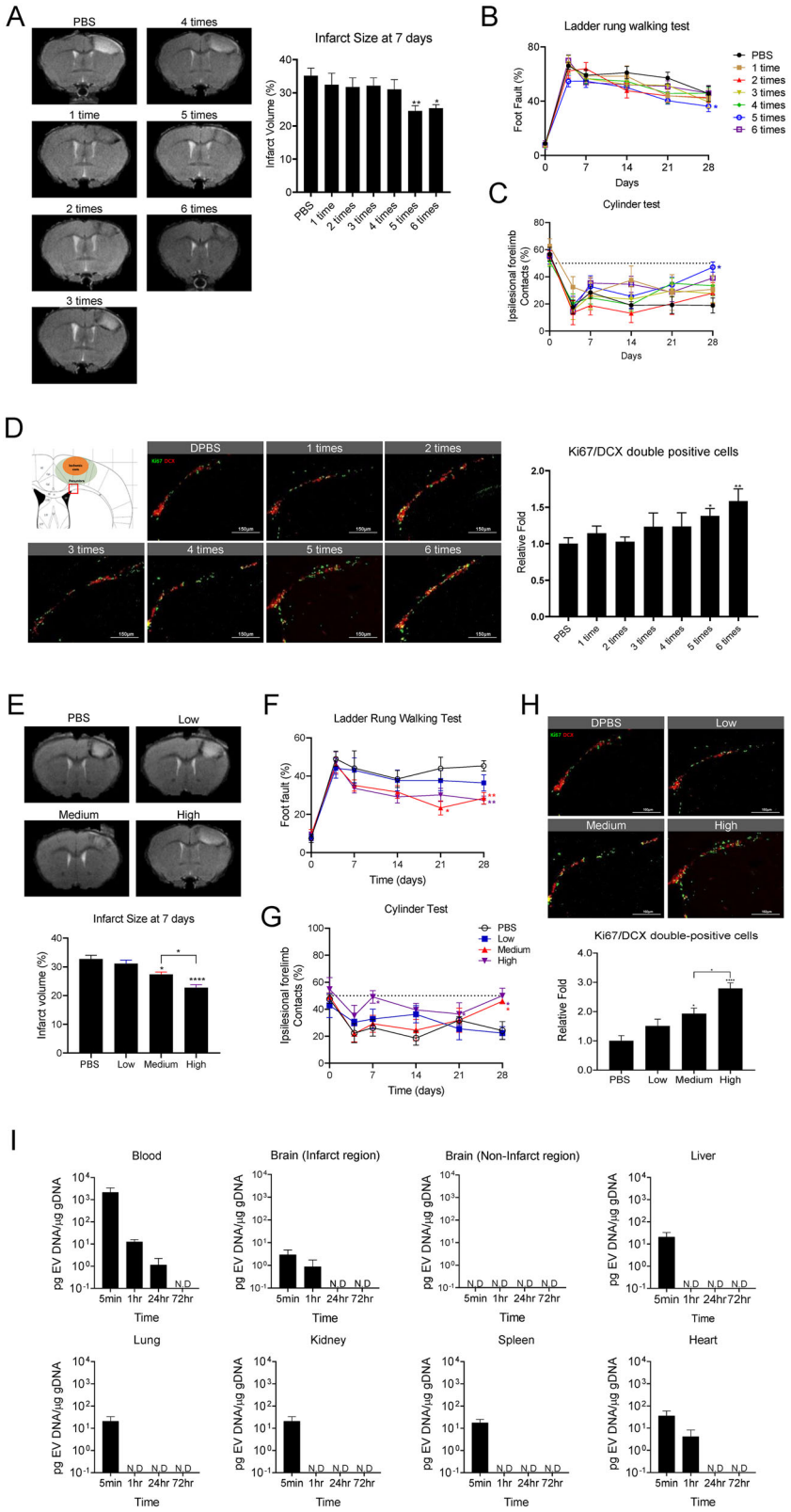

FIGURE 2 | Results of rodent study on the mode and dosage of extracellular vesicles (EVs) treatment and biodistribution in a photothrombotic stroke model.

(A) Effects of EV administration frequency on infarct volume. The images were representative T_2-weighted magnetic resonance imaging (MRI) images at 7 days after photothrombotic (PT) modelling-induced cerebral infarction. The infarct volume on Day 7 was quantified as a ratio relative to the infarct volume observed on Day 1 using the ITK-SNAP software. (B and C) Evaluation of motor function using the ladder walking test (B) and the cylinder test (C) following the administration of EV frequency. (D) Expression of neurogenic marker proteins changes in response to EV administration frequency. Immunofluorescent analysis of neurogenic markers, specifically doublecortin (DCX) and Ki67 proteins. The quantification of double-positive cells for both DCX and Ki67 was performed utilizing QuPath software. The sample sizes for the EV administration frequency (mode) experiments were 8, 5,

20013078, 2025, 6, Downloaded from https://isevjournals.onlinelibrary.wiley.com/doi/10.1002/jev2.70110, Wiley Online Library on [13/01/2026]. See the Terms and Conditions (https://onlinelibrary.wiley.com/terms-and-conditions) on Wiley Online Library for rules of use; OA articles are governed by the applicable Creative Commons License

5, 6, 6, 7 and 5 across the respective groups. (E) Effects of EV administration dose on infarct volume. The images were representative T_2-weighted magnetic resonance imaging (MRI) images at 7 days after photothrombotic (PT) modelling-induced cerebral infarction. The infarct volume on Day 7 was quantified as a ratio relative to the infarct volume observed on Day 1 using the ITK-SNAP software. (F and G) Evaluation of motor function using the ladder walking test (F) and the cylinder test (G) following the administration of EV dose. (H) Expression of neurogenic marker proteins changes in response to EV administration dose. Immunofluorescent analysis of neurogenic markers, specifically doublecortin (DCX) and Ki67 proteins. The quantification of double-positive cells for both DCX and Ki67 was performed utilizing QuPath software. The sample sizes for the EV administration dose (dosage) experiments (E–H) were 6, 7, 7 and 7 across the respective groups. (I) Biodistribution analysis of EVs in a PT stroke mouse model. Tissue samples, along with blood, the infarcted region of the brain, the non-infarcted region of the brain, liver, lung, kidney, spleen and heart, were harvested at 5 min, 1 h, 24 h and 72 h post the final injection of EVs. The data are expressed as mean ± standard error (S.E.). Statistical significance contrasting the PBS group with the EV treatment group is denoted as $*p < 0.05$, $**p < 0.01$, $****p < 0.0001$. The statistical significance among the EV treatment groups is indicated by a dashed line, where $*p < 0.05$.

3.3 | Results of Non-Human Primates

3.3.1 | The Efficacy and Safety of EV Therapeutic in a Marmoset Stroke Model

The therapeutic effects of selected EV dose/frequency were confirmed in a marmoset PT stroke model. For the marmoset stroke model, the treatment dose of EVs was determined using the US FDA conversion guidance documents for industry estimating the maximum safe starting dose in adult healthy volunteers (July 2005). An EV dose of 3.5×10^9 particles per marmoset (equivalent to 6×10^8/mouse) was selected for further experiments of the marmoset PT stroke model. EVs were administered the day after stroke induction for 5 consecutive days (Figure 3A). General symptoms, and changes in body weights and blood tests (haematological and serum biochemical analyses) were serially monitored following the stroke induction and administration of EVs, and there were no statistically significant differences between the EV and control groups (Figure 3B and Tables S4–S5).

To examine the infarct volume and brain microstructural alterations, MRI studies, including T_2-weighted and DTI, were performed at 1, 7, and 28 days after PT stroke. At 7 days, T_2-weighted images showed that infarct size of the EV group was significantly smaller compared to the control group ($p = 0.005$) (Figure 3C). To assess brain microstructural changes, relative fractional anisotropy (FA) and radial diffusivity (RD) values were compared in the internal capsule (IC) and external capsule (EC) regions of interest (ROIs) (Figure 3D). At 7 days, the EV group exhibited significantly higher FA and lower RD values in both the IC ($p = 0.003$ and 0.041, respectively) and EC ($p < 0.001$ and 0.007, respectively) compared to the control group. At 28 days, the EV group showed higher FA and lower RD values in the IC ($p = 0.048$ and 0.033, respectively) compared to the control group.

To evaluate the functional recovery of PT stroke monkeys, behavioural tests including mNSS scoring, grip tests, and Hill and Valley staircase tasks were performed before surgery and at 3, 7, 14, 21, and 28 days after stroke induction (Figure 3E). In the contralesional side assessment, no significant differences were observed between groups in the neurological deficit or grip strength measurements. However, in the ipsilesional side, the EV-treated group showed higher mNSS scores compared to the PBS-treated group at all time points after stroke induction ($p < 0.001$ at 3, 7, and 14 days, $p = 0.026$ at 21 days, and $p = 0.043$ at 28 days). In the grip strength results, the EV group demonstrated higher scores than the control group at Day 3 and 7 ($p < 0.001$ and 0.002, respectively). In the Hill and Valley staircase test, in the ipsilesional side, the EV group performed better than the control group on the tasks at Day 14 ($p = 0.019$) and Day 28 ($p = 0.017$) (Videos S1–S2).

3.4 | Proteomics

After completing the EV efficacy tests, marmoset brain tissues were harvested after 28 days of stroke induction, and proteomic analysis was performed. Normal marmoset brains served as the healthy controls. Proteins were isolated from the brain lesion area, tandem mass tag (TMT) labelled, and LC/MS-MS analysed (Figure 4A). Using the Uniprot DB, 4214 marmoset proteins were identified in the healthy group, 4219 in the control (PBS) group, and 4222 in the EV group. Differentially expressed proteins (DEPs) due to stroke induction (healthy vs. PBS groups) and DEPs due to EV treatment (PBS vs. EV groups) were analysed. Increased DEPs were defined as those satisfying FC (fold change) 1.55 or more/p value 0.1 or less, and decreased DEPs were defined as those satisfying FC 0.64 or less/p value 0.1 or less (Figures 4C–D red dot). A total of 160 DEPs increased by stroke induction, and 43 DEPs were decreased by stroke induction, whereas 39 DEPs were increased by EV treatment, and 21 DEPs were decreased by EV treatment. Among the DEPs commonly identified by stroke induction and EV treatment, 4 proteins were increased by stroke but further increased by EV treatment, 3 proteins were decreased by stroke, but further decreased by EV treatment, 14 proteins were increased by stroke, but decreased after EV treatment, and 32 proteins were decreased by stroke but increased by EV treatment (Figure 4D red dot).

Gene ontology (GO) analysis was performed to identify the function of proteins that were differentially expressed. Gene ontology biological process (GOBP) analysis showed that after stroke induction, the proteins with increased expression were related to immune response and blood coagulation, and the proteins with decreased expression were enriched for genes related to nerve structure and neurosecretion. Compared to stroke, DEPs that increased or decreased by EV treatment were enriched for genes related to neurogenesis and wound healing in GOBP (Figure 4E). Consistent with GO analysis, KEGG pathway enrichment showed that DEPs modulated by stroke and EV treatment were predominantly associated with neurogenesis, immune response, wound repair, and angiogenesis. A comprehensive list of DEPs, including fold changes and adjusted p values, is provided in Table S6. Protein-protein interaction (PPI) networks were analysed

20013078, 2025, 6, Downloaded from https://isevjournals.onlinelibrary.wiley.com/doi/10.1002/jev2.70110, Wiley Online Library on [13/01/2026]. See the Terms and Conditions (https://onlinelibrary.wiley.com/terms-and-conditions) on Wiley Online Library for rules of use; OA articles are governed by the applicable Creative Commons License

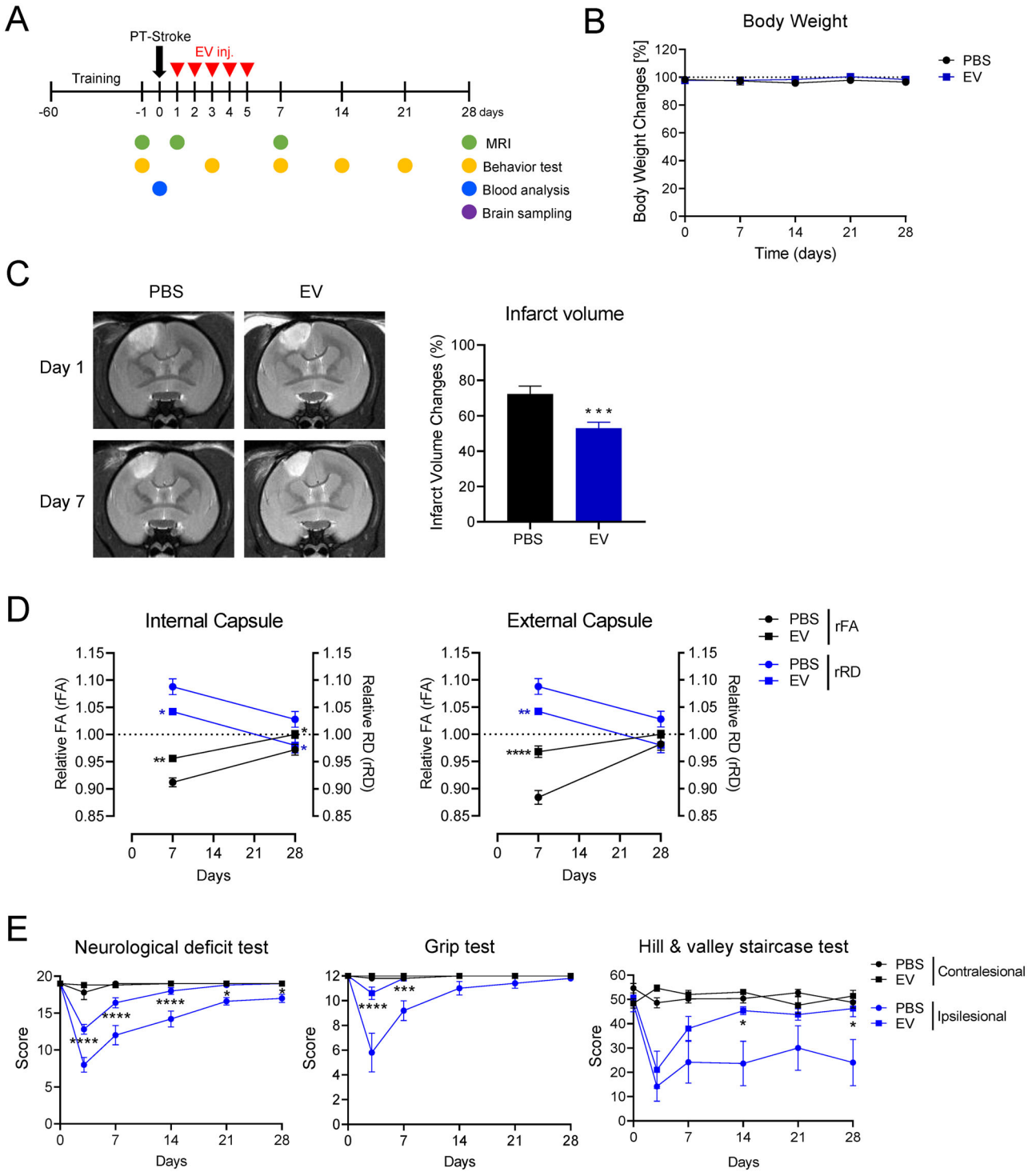

FIGURE 3 | Results of a non-human primate study utilizing a photothrombotic (PT)-induced stroke model in marmosets to evaluate the effects of extracellular vesicle (EV) treatment. (A) Schematic representation of the marmoset experimental design. (B) Variations in body weight observed throughout the experimental duration. (C) The presence of the infarct lesion was identified via T_2-weighted magnetic resonance imaging (MRI) at 1 and 7 days post-PT modelling. (Left panel) Representative image of T_2-weighted MRI scans. (Right panel) Quantitative assessment of infarct volume, calculated as a proportion of the infarct volume on Day 1 using MRIcro software. (D) Alterations in brain microstructure. Diffusion tensor imaging (DTI) was conducted at 7 and 28 days post-PT modelling. The quantitative analysis focused on the relative fractional anisotropy (rFA) and relative fibre density (rFD) within the internal and external capsules. (E) Assessment of behavioural outcomes following EV treatment. Neurological deficit, grip test and hill and valley staircase tests were conducted to evaluate neurological impairments and motor function in both the contralesional and ipsilesional hemispheres. A total of 10 marmosets were utilized in this experimental investigation. Data are expressed as mean ± standard error (SE). Statistical significance comparing the phosphate-buffered saline (PBS) group to the EV treatment group is denoted as follows: $^{*}p < 0.05$, $^{**}p < 0.01$, $^{***}p < 0.001$, $^{****}p < 0.0001$.

20013078, 2025, 6, Downloaded from https://isevjournals.onlinelibrary.wiley.com/doi/10.1002/jev2.70110, Wiley Online Library on [13/01/2026]. See the Terms and Conditions (https://onlinelibrary.wiley.com/terms-and-conditions) on Wiley Online Library for rules of use; OA articles are governed by the applicable Creative Commons License

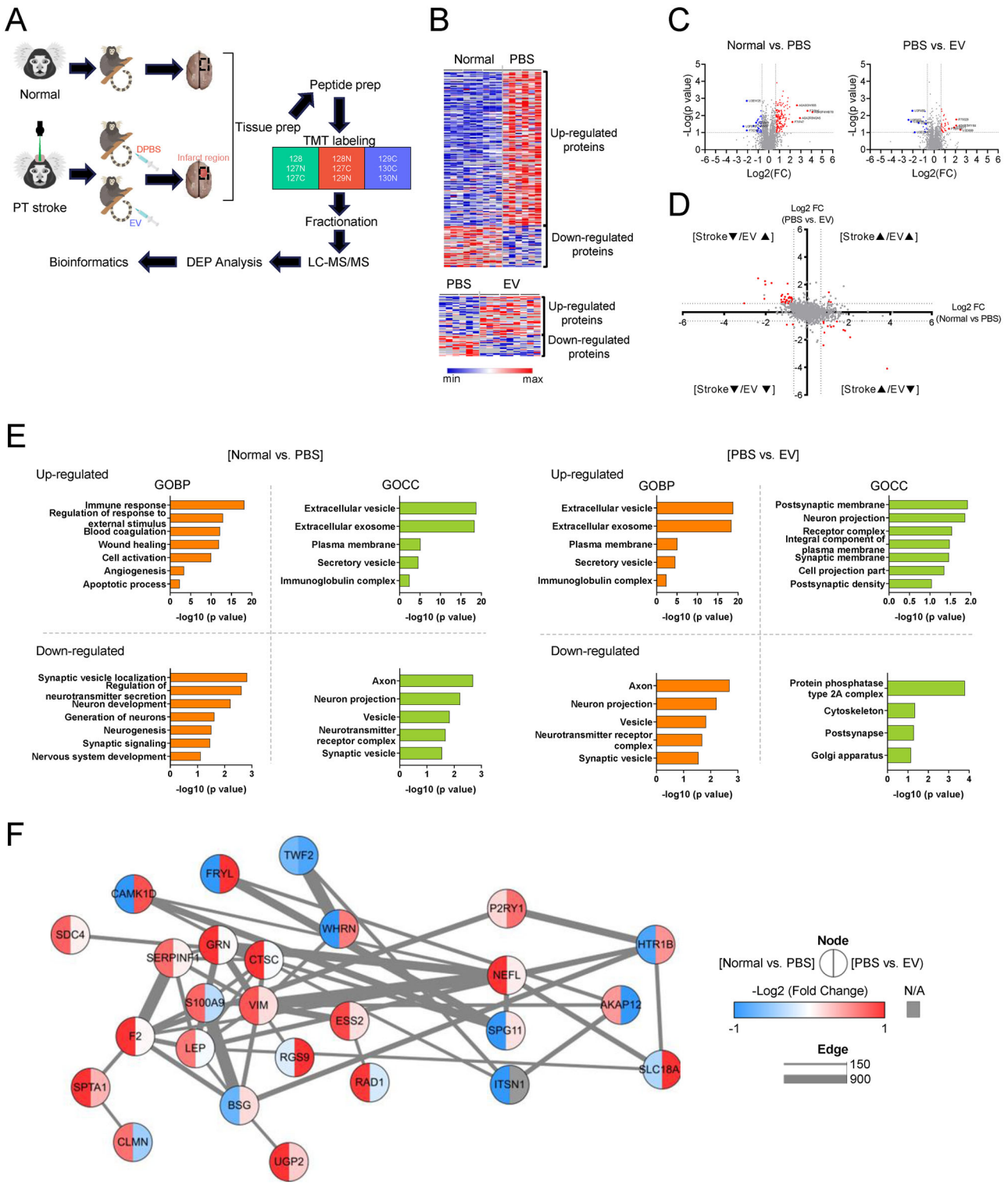

FIGURE 4 | Results of brain proteomics. (A) Framework of marmoset brain proteomics. (B–D) Analysis of differential protein expression. (B) Heatmap representations of differentially expressed proteins (DEPs) comparing the healthy conditions *vs.* phosphate-buffered saline (PBS) groups and the PBS versus EV groups. (C) Volcano plots illustrating the protein variations between the healthy conditions versus PBS groups and the PBS versus EV groups. The red dots indicate upregulated proteins (fold change ≥ 1.55, p value < 0.1), while the blue dots denote downregulated proteins (fold change ≤ 0.64, p value < 0.1). (D) Scatter plot depicting DEPs associated with EV treatment. (E) Gene ontology analysis of DEPs concerning biological processes (GOBP) and cellular components (GOCC). (F) Protein-protein interaction networks of DEPs associated with neural function and neuronal recovery.

20013078, 2025, 6, Downloaded from https://isevjournals.onlinelibrary.wiley.com/doi/10.1002/jev2.70110, Wiley Online Library on [13/01/2026]. See the Terms and Conditions (https://onlinelibrary.wiley.com/terms-and-conditions) on Wiley Online Library for rules of use; OA articles are governed by the applicable Creative Commons License

using DEPs related to neuronal recovery or neural function, which showed that proteins related to neuronal recovery among the proteins affected by EV treatment formed a close network (Figure 4F).

4 | Discussion

MSCs exert their paracrine action in part via EVs in stroke (Zhang et al. 2019). In a randomized trial of MSC treatment in patients with ischaemic stroke, we have demonstrated that intravenous administration of autologous MSCs significantly increases the number of circulating EVs, and select miRNAs incorporated in these EVs were significantly correlated with improvements in motor function and MRI indices of plasticity (Bang et al. 2022). These findings also suggest that the consistency of EV products, in terms of purity and composition, is critical to achieving reproducible therapeutic effects. In the present study, EVs were produced using a 3D bioprocessing platform to ensure scalability and minimize batch variation. The results of characterization of EVs from three different lots demonstrated consistent purity and EV characteristics.

One of the important reasons for failure in clinical trials of new drugs is related to improper selection of dose and dosing frequency, which can lead to ineffective treatment or increased side effects and can ultimately impact the trial's overall success. However, the rationale for EV dose selection and treatment frequency is largely lacking in preclinical studies of EV therapeutics. Gupta et al. examined 64 preclinical studies for EV therapeutics with respect to their applied EV dosing strategies, and found dose discrepancies depending on the disease model, irrespective of the applied EV purification method and cell source (Gupta et al. 2021). As a result, the route and repetition of administration, and dosage of EVs could not be evaluated in clinical trials of EVs (Van Delen et al. 2024). In the present study, we selected the EV dose and dosing frequency using EV particle number and in vivo potency analysis because of limitations of current methods for potency assay and biodistribution of EVs (Gupta et al. 2021; Kang et al. 2021). We found that intravenous administration of 6×10^8 particles/mouse was the minimally effective dose to reduce infarct size and improve recovery after stroke in a mouse PT-stroke model, and the effects were maximized after daily administration for 5 days. The total amount of EVs required for dosing this medium dose for 5 days was 1/10 less compared to that for a single injection of the high dose.

Our present data are in line with previous findings suggesting that fractionated dosing of MSC-EVs over several days yields superior therapeutic effects to a single dose (Nakazaki et al. 2021). In the present study, we accessed the quantitative biodistribution of radio-iodinated (^{125}I) EVs and found that EVs were rapidly cleared from the blood circulation after systemic administration and half-life was not different between single and multiple injections (data not shown). Moreover, in the present study we used recently introduced a novel qPCR-based assay to detect EVs by targeting mitochondrial DNA (Cho et al. 2024), which showed that EVs were rapidly distributed into systemic organs and were relatively specifically distributed to the infarcted brain after repeated daily injection for 5 days. However, an analysis of the effects of EVs from 12 cell sources at three different doses demonstrated that cellular responses to EVs depend on both EV source and EV dose (Hagey et al. 2023). These findings highlight the need for dose-response experiments when evaluating EVs from different cellular origins as therapeutic modalities.

Possible procoagulant properties of MSC-EVs are a safety concern, especially in the case of repeated injection of EVs. EV circulation times decrease after repeated intravenous administration, possibly due to immune response (Driedonks et al. 2022). Our haematological and biochemical analyses showed no changes after repeated EV injections in marmosets, and no immune response was observed in the mixed lymphocyte reaction test (Supplementary Data and Figure S5). To further assess immunogenicity, we evaluated T cell proliferation, apoptosis, and cytokine secretion in PBMCs from healthy donors. While PHA induced strong proliferation in PBMCs and $CD3^+$ T cell subsets, EVs did not elicit a significant response. Similarly, EVs did not increase apoptosis or induce TNF-α or IFN-γ secretion. These findings are consistent with the low immunogenicity of MSC-derived EVs due to minimal MHC expression and lack of nuclear content (Shahir et al. 2020; Bulut and Gürsel 2020; Manzoor et al. 2023). In a 2-week repeated-dose toxicity study in mice, no abnormalities were found in immune-related organs, including the spleen, lymph nodes, and thymus, by gross necropsy or histopathology. Although immune responses to repeated MSC-EV administration are not widely reported, a recent study also showed that VEGF-A mRNA-loaded EVs did not increase immune activation, unlike lipid nanoparticle or adeno-associated virus-based systems (You et al. 2025).

Assessment of functional recovery in non-human primates is important for several reasons. First, loss of hand function is more severe than leg weakness after ischaemic stroke within the territory of the middle cerebral artery, because of larger cortical representation and the need for fine hand motor control. Second, unlike clinical trials for recanalization therapy, in which modified Rankin scale scores of 0–2 (able to walk without assistance) are used for the primary endpoint for favourable effects, more detailed motor assessments including hand function are needed for preclinical and clinical trials of cell therapy or MSC-EV therapeutics (Savitz et al. 2011). The non-human primate models enable the evaluation of fine motor function of the hand and can aid in distinguishing compensatory recovery, which commonly occurs after stroke, from true recovery. For these reasons, many researchers have conducted functional assessments using non-human primates when evaluating the therapeutic effects of MSC-EVs in stroke models (Moore et al. 2019; Go et al. 2020, 2021). In the present study, behavioural test of non-human primates using standardized tests showed that not only global behavioural functions but also fine hand function recovered after treatment of our EV therapeutic.

In addition, spontaneous recovery is common in patients with stroke. For this reason, many clinical trials for new stroke drugs have failed to achieve significant results. Previous immunohistochemistry studies in primates have reported that recovery of hand function is associated with anatomical rewiring after injury (Dancause et al. 2005; Darling et al. 2018). Neuroimaging biomarkers can serve as objective measures, providing accurate and reliable assessment of treatment outcomes. Morphological changes by MRI can be sensitive indicators of neuroprotec-

20013078, 2025, 6, Downloaded from https://isevjournals.onlinelibrary.wiley.com/doi/10.1002/jev2.70110, Wiley Online Library on [13/01/2026]. See the Terms and Conditions (https://onlinelibrary.wiley.com/terms-and-conditions) on Wiley Online Library for rules of use; OA articles are governed by the applicable Creative Commons License

tion after ischaemic brain damage, while brain microstructural connectivity alterations measured by DTI have been used to evaluate functional recovery in neurological diseases (Son et al. 2021). The present study showed that EV therapy reduced infarct lesion volume after stroke. DTI measures the degree of the anisotropic diffusion of water molecules in the brain using a diffusion-encoded gradient (Tournier et al. 2011). FA values, which are associated with neural fibre tract integrity, are used to investigate recovery after ischaemic stroke (Otero-Ortega et al. 2017). With the DTI index and DTT-derived rFD values, our results of DTI measurements indicate therapy-induced axonal remodelling after ischaemia in the non-human primate stroke model. Several preclinical studies evaluated the effects of MSC-EV therapeutics in non-human primates in stroke or traumatic brain injury (Go et al. 2021; Medalla et al. 2020; Zhou et al. 2023). To our knowledge, this is the first study of a clinical scale MSC-EV therapeutic in a stroke model of non-human primates evaluated using standardized clinically relevant tests for functional and neuroimaging recovery after stroke.

Proteomics is the large-scale study of proteins, including their expression, functions, and interactions within a biological context. In our non-human primate stroke model, EV treatment altered a select group of proteins, such as ZMYND8, CTSC, SPINT1, CLMN, and AKAP12, which are associated with neurogenesis, angiogenesis, synaptic signalling, and brain repair processes. For instance, ZMYND8 (zinc finger MYND-type containing 8) and SPINT1 (serine peptidase inhibitor, Kunitz unit 1) regulate neural differentiation (Adhikary et al. 2022; Guha et al. 2024; Koivuniemi et al. 2013), CLMN is involved in neurite outgrowth (Marzinke and Clagett-Dame 2012), CTSC (cathepsin C) influences inflammation and angiogenesis (Chalmers et al. 2023; Hagemann et al. 2021), and AKAP12 (A-kinase anchoring protein 12) supports synaptic plasticity and blood-brain barrier integrity (Kimura et al. 2023). Using target gene prediction database analysis, ZMYND8 and CTSC were identified as possible direct target genes of miR-27a-3p and miR-132-3p, which are enriched in our EV therapeutic (SNE-101) and mediate molecular functions associated with neurogenesis (Son et al. 2023). SPINT1, CLMN, and AKAP12 are direct target genes of miR-92a-3p, miR-181b-3p, and miR-210-3p, which are enriched in our EVs. These results suggest that EVs facilitate motor recovery and cortical microstructure repair by modulating key proteins involved in neuroplasticity and brain remodelling, beyond natural recovery after stroke.

The strengths of this study include (a) the clinical scale MSC-EV therapeutic used in this study was produced and isolated at a GMP facility. All processes were performed according to the current guidelines on quality, non-clinical and clinical assessment of EV therapy products of the Korean Food and Drug Administration (released 2018 and 2023), and using GMP-compliant methods; (b) experiments in non-human primates (marmosets), using standardized tests and the same study protocol as rodent studies (Le Gal et al. 2018); and (c) objective measurements of neuroplasticity were performed using MRI to investigate mechanisms underlying MSC-EV-induced recovery after stroke.

However, several limitations deserve to be mentioned. (a) Our analysis of the EV effects showed that our EVs were enriched with miRNAs, which mediate neurite growth of neural progenitor/stem cells (Son et al. 2023). Although genetic profiling is more similar between humans and non-human primates than between humans and rodents, there exist non-conserved miRNAs regulating neural processes as well as significant differences in the expression levels of miRNAs and target genes in the brains of humans and non-human primates (McCreight et al. 2017; Hu et al. 2011). However, the miRNAs associated with the key therapeutic effects of MSC-EVs are conserved across humans, non-human primates, and rodents (Son et al. 2023). (b) The differences between experimental animal stroke models and ischaemic stroke in humans may contribute to the discrepancy between preclinical and clinical results (Elkins et al. 2017). In the present study, PT-stroke model was used in both mice and non-human primates to evaluate the effects of EVs on functional recovery and improvement of connectivity on neuroimaging after stroke. The PT-stroke model represents cortical infarcts without reperfusion, which is the most common type of non-lacunar stroke in patients with acute ischaemic stroke and is suitable for the evaluation of the effects of neurorestorative treatment, while the transient middle cerebral artery occlusion (tMCAo) suture model is the most widely used model for preclinical studies for recanalization and neuroprotection therapies. The PT-stroke model is increasingly being used for the experimental treatment of stroke, including MSC-EV therapeutics, due to a higher reproducibility and a lower mortality, compared to the tMCAo suture model. We previously showed that an EV therapeutic has effects on both the rat tMCAo suture model and the mice PT-stroke model (Son et al. 2023).

Another limitation of this study is the inability to quantify the percentage of injected dose (%ID) of EVs, particularly within the infarcted brain. Although lipid-friendly fluorescent dyes like PKH67, PKH26, and DiI are widely used for EV tracking due to their simplicity and sensitivity (Chen et al. 2023), they have notable drawbacks. These dyes can form micelles indistinguishable from EVs, and inadequate removal of free dye may cause false distribution patterns. Moreover, dyes may transfer to cell membranes after EV uptake, and their slow degradation can lead to long-term artefacts in organs such as the liver, kidney, and spleen (Simonsen 2019). Thus, fluorescent signals may not accurately represent true EV localization. To address these issues, we employed a recently developed method targeting EV-associated mtDNA, which allows for more precise quantification without dyes (Cho et al. 2024). However, even this approach has limitations, especially under pathological conditions like stroke, where tissue damage and inflammation can affect %ID measurements. Therefore, accurate evaluation of EV biodistribution requires integrated analytical strategies combining multiple complementary methods.

In summary, our present study indicates that systemic administration of SNE-101, a clinical scale EV therapeutic, accelerates neurological recovery, including hand functions, in a non-human primate PT-stroke model when EVs were administrated with the selected dose and time frequency. Neuroimaging biomarkers and proteomics analysis suggested that this effect is related to enhanced neuroplasticity by increasing the level of proteins related to the development and function of the nervous system. Our data support that MSC-EV therapeutics should be viewed as a promising therapeutic strategy for functional recovery after stroke with great potential for clinical applications. To this end, a Phase

20013078, 2025, 6, Downloaded from https://isevjournals.onlinelibrary.wiley.com/doi/10.1002/jev2.70110, Wiley Online Library on [13/01/2026]. See the Terms and Conditions (https://onlinelibrary.wiley.com/terms-and-conditions) on Wiley Online Library for rules of use; OA articles are governed by the applicable Creative Commons License

1b trial (STem cell-derived Extracellular Vesicle therapy In Acute ischemic stroke [STEVIA]; ClinicalTrials.gov ID: NCT06995625) will evaluate the safety, dose-limiting toxicity, and preliminary efficacy of intravenously administered SNE-101 in patients with acute ischemic stroke.

Author Contributions

Eun Hee Kim: conceptualization (lead), data curation (lead), formal analysis (lead), investigation (lead), methodology (lead), validation (lead), visualization (lead), writing – original draft (lead), writing – review and editing (lead). **Jeong Pyo Son**: conceptualization (lead), data curation (lead), formal analysis (lead), investigation (lead), methodology (lead), validation (lead), visualization (lead), writing – original draft (lead), writing – review and editing (lead). **Gyun Sik Oh**: investigation (supporting), methodology (supporting). **Suji Park**: investigation (supporting), methodology (supporting). **Eunchong Hong**: investigation (supporting), methodology (supporting). **Kyoung-Sun Lee**: investigation (supporting), methodology (supporting). **Michael Chopp**: conceptualization (equal), methodology (equal), supervision (equal), writing – review and editing (equal). **Oh Young Bang**: conceptualization (lead), funding acquisition (lead), investigation (lead), resources (lead), supervision (lead), validation (lead), visualization (lead), writing – original draft (lead), writing – review and editing (lead).

Conflicts of Interest

The authors of this manuscript have the following competing interests: Eun Hee Kim, Gyun Sik Oh, and Suji Park are paid employees of S&E bio Co., Ltd. S&E bio Co., Ltd. have filed a patent application related to the methods described in this study, but there is no marketing product to declare. This does not affect our adherence to the data and material-sharing policies of the Journal of Extracellular Vesicles.

Data Availability Statement

The data that support the findings of this study are available from the corresponding author upon reasonable request.

References

Adhikary, S., V. Singh, R. Choudhari, et al. 2022. "ZMYND8 Suppresses MAPT213 LncRNA Transcription to Promote Neuronal Differentiation." *Cell Death & Disease* 13, no. 9: 766.

Bang, O. Y., E. H. Kim, Y. H. Cho, et al. 2022. "Circulating Extracellular Vesicles in Stroke Patients Treated With Mesenchymal Stem Cells: A Biomarker Analysis of a Randomized Trial." *Stroke* 53, no. 7: 2276–2286.

Bulut, O., and İ. Gürsel. 2020. "Mesenchymal Stem Cell Derived Extracellular Vesicles: Promising Immunomodulators Against Autoimmune, Autoinflammatory Disorders and SARS-CoV-2 Infection." *Turkish Journal of Biology* 44, no. 7: 273–282.

Chalmers, J. D., R. Kettritz, and B. Korkmaz. 2023. "Dipeptidyl Peptidase 1 Inhibition as a Potential Therapeutic Approach in Neutrophil-Mediated Inflammatory Disease." *Frontiers in Immunology* 14: 1239151.

Chen, C., N. Cai, Q. Niu, Y. Tian, Y. Hu, and X. Yan. 2023. "Quantitative Assessment of Lipophilic Membrane Dye-Based Labelling of Extracellular Vesicles by Nano-Flow Cytometry." *Journal of Extracellular Vesicles* 12, no. 8: 12351.

Cho, Y. W., M. Y. Cho, J. Yoon, et al. 2024. "Evaluation of Unmodified Human Cell-Derived Extracellular Vesicle Mitochondrial Deoxyribonucleic Acid-Based Biodistribution in Rodents." *Journal of Extracellular Vesicles* 13, no. 7: e12489.

Cook, D. J., L. Teves, and M. Tymianski. 2012. "Treatment of Stroke With a PSD-95 Inhibitor in the Gyrencephalic Primate Brain." *Nature* 483, no. 7388: 213–217.

Welsh, J. A., D. C. I. Goberdhan, L. O'Driscoll, et al. 2024. "Minimal Information for Studies of Extracellular Vesicles (MISEV2023): From Basic to Advanced Approaches." *Journal of Extracellular Vesicles* 13, no. 2: e12404.

Dancause, N., S. Barbay, S. B. Frost, et al. 2005. "Extensive Cortical Rewiring After Brain Injury." *Journal of Neuroscience* 25, no. 44: 10167–10179.

Darling, W. G., J. Ge, K. S. Stilwell-Morecraft, D. L. Rotella, M. A. Pizzimenti, and R. J. Morecraft. 2018. "Hand Motor Recovery Following Extensive Frontoparietal Cortical Injury Is Accompanied by Upregulated Corticoreticular Projections in Monkey." *Journal of Neuroscience* 38, no. 28: 6323–6339.

Dirnagl, U., A. Hakim, M. Macleod, et al. 2013. "A Concerted Appeal for International Cooperation in Preclinical Stroke Research." *Stroke: A Journal of Cerebral Circulation* 44, no. 6: 1754–1760.

Doeppner, T. R., J. Herz, A. Görgens, et al. 2015. "Extracellular Vesicles Improve Post-Stroke Neuroregeneration and Prevent Postischemic Immunosuppression." *Stem Cells Translational Medicine* 4, no. 10: 1131–1143.

Driedonks, T., L. Jiang, B. Carlson, et al. 2022. "Pharmacokinetics and Biodistribution of Extracellular Vesicles Administered Intravenously and Intranasally to Macaca Nemestrina." *Journal of Extracellular Biology* 1, no. 10: e59.

Elkins, J., R. Veltkamp, J. Montaner, et al. 2017. "Safety and Efficacy of Natalizumab in Patients With Acute Ischaemic Stroke (ACTION): A Randomised, Placebo-Controlled, Double-Blind Phase 2 Trial." *Lancet Neurology* 16, no. 3: 217–226.

Fisher, M. 2011. "New Approaches to Neuroprotective Drug Development." *Supplement, Stroke: A Journal of Cerebral Circulation* 42, no. S1: S24–S27.

Go, V., B. G. Bowley, M. A. Pessina, et al. 2020. "Extracellular Vesicles From Mesenchymal Stem Cells Reduce Microglial-Mediated Neuroinflammation After Cortical Injury in Aged Rhesus Monkeys." *Geroscience* 42: 1–17.

Go, V., D. Sarikaya, Y. Zhou, et al. 2021. "Extracellular Vesicles Derived From Bone Marrow Mesenchymal Stem Cells Enhance Myelin Maintenance After Cortical Injury in Aged Rhesus Monkeys." *Experimental Neurology* 337: 113540.

Guha, D., V. Singh, S. Nandi, E. I. Ramos, S. S. Gadad, and C. Das. 2024. "ZMYND8 Is a Regulator of Sonic Hedgehog Signaling in ATRA-Mediated Differentiation of Neuroblastoma Cells." *Biochemistry* 63, no. 12: 1534–1542.

Gupta, D., A. M. Zickler, and S. El Andaloussi. 2021. "Dosing Extracellular Vesicles." *Advanced Drug Delivery Reviews* 178: 113961.

Hagemann, N., P. Ludewig, M. Gunzer, A. M. Yusuf, and D. M. Hermann. 2021. "Roles of Polymorphonuclear Neutrophils in Ischemic Brain Injury and Post-Ischemic Brain Remodeling." *Frontiers in Immunology* 12: 825572.

Hagey, D. W., M. Ojansivu, B. R. Bostancioglu, et al. 2023. "The Cellular Response to Extracellular Vesicles Is Dependent on Their Cell Source and Dose." *Science Advances* 9, no. 35: eadh1168.

Hill, M. D., M. Goyal, B. K. Menon, et al. 2020. "Efficacy and Safety of Nerinetide for the Treatment of Acute Ischaemic Stroke (ESCAPE-NA1): A Multicentre, Double-Blind, Randomised Controlled Trial." *Lancet* 395, no. 10227: 878–887.

Hossmann, K. A. 2012. "The Two Pathophysiologies of Focal Brain Ischemia: Implications for Translational Stroke Research." *Journal of Cerebral Blood Flow and Metabolism* 32, no. 7: 1310–1316.

Hu, H. Y., S. Guo, J. Xi, et al. 2011. "MicroRNA Expression and Regulation in Human, Chimpanzee, and Macaque Brains." *PLoS Genetics* 7, no. 10: e1002327.

Hua, Y., T. Schallert, R. F. Keep, J. Wu, J. T. Hoff, and G. Xi. 2002. "Behavioral Tests After Intracerebral Hemorrhage in the Rat." *Stroke: A Journal of Cerebral Circulation* 33, no. 10: 2478–2484.

20013078, 2025, 6, Downloaded from https://isevjournals.onlinelibrary.wiley.com/doi/10.1002/jev2.70110, Wiley Online Library on [13/01/2026]. See the Terms and Conditions (https://onlinelibrary.wiley.com/terms-and-conditions) on Wiley Online Library for rules of use; OA articles are governed by the applicable Creative Commons License

Kang, M., V. Jordan, C. Blenkiron, and L. W. Chamley. 2021. "Biodistribution of Extracellular Vesicles Following Administration Into Animals: A Systematic Review." *Journal of Extracellular Vesicles* 10, no. 8: e12085.

Kilkenny, C., W. J. Browne, I. C. Cuthill, M. Emerson, and D. G. Altman. 2010. "Improving Bioscience Research Reporting: The ARRIVE Guidelines for Reporting Animal Research." *PloS Biology* 8, no. 6: e1000412.

Kimura, S., J. Lok, I. H. Gelman, E. H. Lo, and K. Arai. 2023. "Role of A-Kinase Anchoring Protein 12 in the Central Nervous System." *Journal of Clinical Neurology* 19, no. 4: 329–337.

Koivuniemi, R., J. Makela, M. E. Hokkane, et al. 2013. "Hepatocyte Growth Factor Activator Inhibitor-1 Is Induced by Bone Morphogenetic Proteins and Regulates Proliferation and Cell Fate of Neural Progenitor Cells." *PLoS ONE* 8, no. 2: e56117.

Le Friec, A., F. Desmoulin, and B. Demain, et al. 2021. "A Reproducible New Model of Focal Ischemic Injury in the Marmoset Monkey: MRI and Behavioural Follow-Up." *Translational Stroke Research* 12: 98–111.

Le Gal, R., M. Bernaudin, J. Toutain, and O. Touzani. 2018. "Assessment of Behavioural Deficits Following Ischaemic Stroke in the Marmoset." *Behavioural Brain Research* 352: 151–160.

Medalla, M., W. Chang, S. M. Calderazzo, et al. 2020. "Treatment With Mesenchymal-Derived Extracellular Vesicles Reduces Injury-Related Pathology in Pyramidal Neurons of Monkey Perilesional Ventral Premotor Cortex." *Journal of Neuroscience: The Official Journal of the Society for Neuroscience* 40, no. 17: 3385–3407.

Marzinke, M. A., and M. Clagett-Dame. 2012. "The All-Trans Retinoic Acid (atRA)-Regulated Gene Calmin (Clmn) Regulates Cell Cycle Exit and Neurite Outgrowth in Murine Neuroblastoma (Neuro2a) Cells." *Experimental Cell Research* 318, no. 1: 85–93.

McCreight, J. C., S. E. Schneider, D. B. Wilburn, and W. J. Swanson. 2017. "Evolution of microRNA in Primates." *PLoS ONE* 12, no. 6: e0176596.

Manzoor, T., A. Saleem, N. Farooq, et al. 2023. "Extracellular Vesicles Derived From Mesenchymal Stem Cells—A Novel Therapeutic Tool in Infectious Diseases." *Inflammation and Regeneration* 43, no. 1: 17.

Metz, G. A., and I. Q. Whishaw. 2002. "Cortical and Subcortical Lesions Impair Skilled Walking in the Ladder Rung Walking Test: A New Task to Evaluate Fore-and Hindlimb Stepping, Placing, and Co-Ordination." *Journal of Neuroscience Methods* 115, no. 2: 169–179.

Molina, C. A. 2010. "Futile Recanalization in Mechanical Embolectomy Trials: a Call to Improve Selection of Patients for Revascularization." *Stroke: A Journal of Cerebral Circulation* 41, no. 5: 842–843.

Moon, G. J., J. H. Sung, D. H. Kim, et al. 2019. "Application of Mesenchymal Stem Cell-Derived Extracellular Vesicles for Stroke: Biodistribution and microRNA Study." *Translational Stroke Research* 10: 509–521.

Moore, T., B. Bowley, M. Pessina, et al. 2019. "Mesenchymal Derived Exosomes Enhance Recovery of Motor Function in a Monkey Model of Cortical Injury." *Restorative Neurology and Neuroscience* 37, no. 4: 347–362.

Nakazaki, M., T. Morita, K. L. Lankford, P. W. Askenase, and J. D. Kocsis. 2021. "Small Extracellular Vesicles Released by Infused Mesenchymal Stromal Cells Target M2 Macrophages and Promote TGF-Beta Upregulation, Microvascular Stabilization and Functional Recovery in a Rodent Model of Severe Spinal Cord Injury." *Journal of Extracellular Vesicles* 10, no. 11: e12137.

O'Collins, V. E., M. R. Macleod, G. A. Donnan, L. L. Horky, B. H. van der Worp, and D. W. Howells. 2006. "1,026 Experimental Treatments in Acute Stroke." *Annals of Neurology* 59, no. 3: 467–477.

Otero-Ortega, L., F. Laso-Garcia, and M. D. Gomez-de Frutos, et al. 2017. "White Matter Repair After Extracellular Vesicles Administration in an Experimental Animal Model of Subcortical Stroke." *Scientific Reports* 7: 44433.

Powers, W. J., A. A. Rabinstein, T. Ackerson, et al. 2019. "Guidelines for the Early Management of Patients With Acute Ischemic Stroke: 2019 Update to the 2018 Guidelines for the Early Management of Acute Ischemic Stroke: A Guideline for Healthcare Professionals From the American Heart Association/American Stroke Association." *Stroke: A Journal of Cerebral Circulation* 50, no. 12: e344–e418.

Ribo, M., J. Alvarez-Sabin, J. Montaner, et al. 2006. "Temporal Profile of Recanalization After Intravenous Tissue Plasminogen Activator: Selecting Patients for Rescue Reperfusion Techniques." *Stroke: A Journal of Cerebral Circulation* 37, no. 4: 1000–1004.

Savitz, S. I., M. Chopp, R. Deans, et al. 2011. "Stem Cell Therapy as an Emerging Paradigm for Stroke (STEPS) II." *Stroke* 42, no. 3: 825–829.

Shahir, M., S. M. Hashemi, A. Asadirad, et al. 2020. "Effect of Mesenchymal Stem Cell-Derived Exosomes on the Induction of Mouse Tolerogenic Dendritic Cells." *Journal of Cellular Physiology* 235, no. 10: 7043–7055.

Simonsen, J. B. 2019. "Pitfalls Associated With Lipophilic Fluorophore Staining of Extracellular Vesicles for Uptake Studies." *Journal of Extracellular Vesicles* 8, no. 1: 1582237.

Son, J. P., E. H. Kim, E. K. Shin, et al. 2023. "Mesenchymal Stem Cell-Extracellular Vesicle Therapy for Stroke: Scalable Production and Imaging Biomarker Studies." *Stem Cells Translational Medicine* 12, no. 7: 459–473.

Son, J. P., J. H. Sung, D. H. Kim, et al. 2021. "Brain Morphological and Connectivity Changes on MRI After Stem Cell Therapy in a Rat Stroke Model." *PLoS ONE* 16, no. 2: e0246817.

Tardif, S. D., K. G. Mansfield, R. Ratnam, C. N. Ross, and T. E. Ziegler. 2011. "The Marmoset as a Model of Aging and Age-related Diseases." *ILAR Journal* 52, no. 1: 54–65.

Thery, C., K. W. Witwer, E. Aikawa, et al. 2018. "Minimal Information for Studies of Extracellular Vesicles 2018 (MISEV2018): A Position Statement of the International Society for Extracellular Vesicles and Update of the MISEV2014 Guidelines." *Journal of Extracellular Vesicles* 7, no. 1: 1535750.

Tournier, J. D., S. Mori, and A. Leemans. 2011. "Diffusion Tensor Imaging and Beyond." *Magnetic Resonance in Medicine: Official Journal of the Society of Magnetic Resonance in Medicine /Society of Magnetic Resonance in Medicine* 65, no. 6: 1532–1556.

Tymianski, M. 2011. "Emerging Mechanisms of Disrupted Cellular Signaling in Brain Ischemia." *Nature Neuroscience* 14, no. 11: 1369–1373.

Van Delen, M., J. Derdelinckx, K. Wouters, I. Nelissen, and N. Cools. 2024. "Systematic Review and Meta-Analysis of Clinical Trials Assessing Safety and Efficacy of Human Extracellular Vesicle-Based Therapy." *Journal of Extracellular Vesicles* 13, no. 7: e12458.

Xin, H., Y. Li, B. Buller, et al. 2012. "Exosome-Mediated Transfer of miR-133b From Multipotent Mesenchymal Stromal Cells to Neural Cells Contributes to Neurite Outgrowth." *Stem Cells* 30, no. 7: 1556–1564.

You, Y., Y. Tian, R. Guo, et al. 2025. "Extracellular Vesicle-Mediated VEGF-A mRNA Delivery Rescues Ischaemic Injury With Low Immunogenicity." *European Heart Journal* 46, no. 17: 1662–1676.

Zhang, Z. G., B. Buller, and M. Chopp. 2019. "Exosomes—Beyond Stem Cells for Restorative Therapy in Stroke and Neurological Injury." *Nature Reviews Neurology* 15, no. 4: 193–203.

Zhou, Y., H. Bhatt, C. A. Mojica, et al. 2023. "Mesenchymal-Derived Extracellular Vesicles Enhance Microglia-Mediated Synapse Remodeling After Cortical Injury in Aging Rhesus Monkeys." *Journal of Neuroinflammation* 20, no. 1: 201.

Supporting Information

Additional supporting information can be found online in the Supporting Information section.

Supplementary data: jev270110-sup-0003-SuppMat.docx **Supplementary Video 1**: jev270110-vid-0001-VideoS1.mp4 **Supplementary Video 2**: jev270110-vid-0002-VideoS1.mp4

20013078, 2025, 6, Downloaded from https://isevjournals.onlinelibrary.wiley.com/doi/10.1002/jev2.70110, Wiley Online Library on [13/01/2026]. See the Terms and Conditions (https://onlinelibrary.wiley.com/terms-and-conditions) on Wiley Online Library for rules of use; OA articles are governed by the applicable Creative Commons License